Zigzag instability of biased pusher swimmers

ERIC LAUGA[1](a) (iD) , THANH NGHI DANG[2,3] and TAKUJI ISHIKAWA[2](b) (iD)

[1] *Department of Applied Mathematics and Theoretical Physics, University of Cambridge - Cambridge CB3 0WA, UK*
[2] *Department of Finemechanics, Graduate School of Engineering, Tohoku University - 6-6-01, Aoba, Aoba-ku, Sendai 980-8579, Japan*
[3] *Faculty of Mechanical Engineering, RWTH Aachen University - 52056 Aachen, Germany*

Abstract – Microorganisms self-propelling in a fluid create flow fields that impact the dynamics of other swimmers. Some organisms can be biased and have a preferred swimming direction, *e.g.*, those displaying gyrotaxis, chemotaxis or phototaxis, and as a result often focus along thin lines. Here we use numerical computations and far-field theoretical calculations to show that the position of a collection of biased swimmers moving along a line is unstable to a zigzag mode when the swimmers act on the fluid as pusher dipoles. This instability takes the form of periodic transverse oscillations in the position of the swimmers. We predict theoretically that the most unstable wavelength is equal to twice the inter-swimmer distance and that the growth rate of the instability increases linearly with the magnitude of the stresslet, both of which are in quantitative agreement with our numerical simulations.

Introduction. – The swimming of biological microorganisms is a rich field of study, encompassing under the same umbrella a wide range of species, from simple unicellular bacteria to large eukaryotes and multicellular aquatic organisms [1]. From the point of view of physics, over seventy years of work since GI Taylor's early paper [2] has led to significant advances in our understanding of the required symmetry breaking at the cellular level [3], the fluid dynamics governing the flows around the cells [4,5] and the physics of active matter [6].

As a microorganism self-propels in a fluid using its appendages, *e.g.*, flagella or cilia, it creates long-range flows. Since microswimmers are force free, the flow fields are typically force dipoles, known more generally in hydrodynamics as stresslets [7] and decaying spatially with distance r as $1/r^2$. The stresslets of swimmers are of two types: "pusher", for cells pushed from the back by their flagella and "puller" in the opposite case where the cell is being pulled from its beating appendages located in front of it [5]. These flows have been measured and, except for dense multicellular organisms that exert localised forces [8], experimental agreement with the stresslet model is excellent far from the swimming organism [9]. When the

swimming motion is time varying, the nearby flows can alternate between pusher and puller modes [10] and include additional complexity [8,11].

The flow fields created by the moving cells can impact the dynamics of other nearby swimmers and hydrodynamic interactions have been shown to affect the coupled locomotion of swimmers [12–14]. At the level of a population of cells, this can then induce new, collective modes of locomotion [15–17], impact fluid rheology [18] and lead to bio-inspired dynamics in artificial colloids [19]. Experimental work on bacteria in their swimming [20–24] or swarming states [25,26], algae [27,28] and spermatozoa [29,30] provide diverse examples of correlated, collective dynamics mediated by the surrounding fluid. Collective effects have also been addressed from the point of view of statistical physics [31,32].

Analogous to the classical route used to understand the transition to turbulence [33], one method to tackle the fundamental hydrodynamics of collective locomotion consists in looking for unstable modes to fixed points of the coupled cell dynamics. Pioneering work showed that long-wavelength perturbations to any ordered swimmer suspensions are unstable [34], which can be rationalised by inspecting the vorticity created by stresslets [5]. Homogeneous dilute suspensions of pusher swimmers were also

(a)E-mail: e.lauga@damtp.cam.ac.uk
(b)E-mail: t.ishikawa@tohoku.ac.jp

shown to be unstable in orientation while pullers were predicted to remain stable [35,36]. Recent work addressed instabilities in artificial swimmers [37].

In this letter, we consider a collection of pusher swimmers assumed to be biased to swim in a particular direction. This setup is relevant to a wide range of biological situations, with a bias that could arise from many external factors. For example, some aquatic organisms are bottom heavy so they display gravitaxis and are passively reoriented to swim upwards [38]. Similarly, swimmers displaying phototaxis reorient themselves and swim toward light sources [39,40] while cells undergoing chemotaxis [41,42] may also be modelled empirically as being biased in their orientation.

In these cases where swimming is biased in a particular direction, cells subject to an external flow acting in the direction opposite to the preferred swimming direction are known to focus along elongated threads; this focusing phenomenon was originally demonstrated in the case of bottom-heavy algae in pipe flow [43]. Lines of such swimmers were then shown to be subject to a clustering instability in the case of puller swimmers, while pushers remained stable [44]. In this letter, we use a combination of numerical computations and far-field theoretical calculations to show that a collection of biased pusher cells swimming along a line is unstable to transverse perturbations in the position of the swimmers. We predict theoretically that the most unstable mode has a wavelength equal to twice the distance between swimmers (zigzag mode) and that its growth rate increases linearly with the magnitude of the stresslet, both of which are in quantitative agreement with our numerical simulations.

We first present in an overview of our numerical methods along with the results of our simulations. We then use a far-field theoretical model to study the instability, and compare the theoretical results with those of the computations. We conclude by a discussion and a summary of our results.

Numerical simulations. –

Setup. The classical model swimmer used in this study is the spherical squirmer [45,46]. The swimmer is assumed to be neutrally buoyant, non-Brownian and to swim at a very small Reynolds number. To include the bias in its locomotion we make the swimmer bottom heavy, which adds a restoring gravitational torque every time it is not aligned vertically pointing upwards. The presence of this restoring torque allows us then to model all cases where the swimmer is biased to swim in a particular direction, not just that due to gravitaxis.

In the squirmer model, the surface of the spherical cell is prescribed to move purely tangentially, with a tangential motion assumed to be axisymmetric and time independent. We denote by $\mathbf{e}$ the unit orientation vector in the direction of swimming. Using spherical coordinates, we follow ref. [12], and prescribe the tangential surface velocity, $\mathbf{u}_s$, as $\mathbf{u}_s = (3U_0/2)(\sin\theta + \beta\sin\theta\cos\theta)\mathbf{e}_\theta$, where U_0
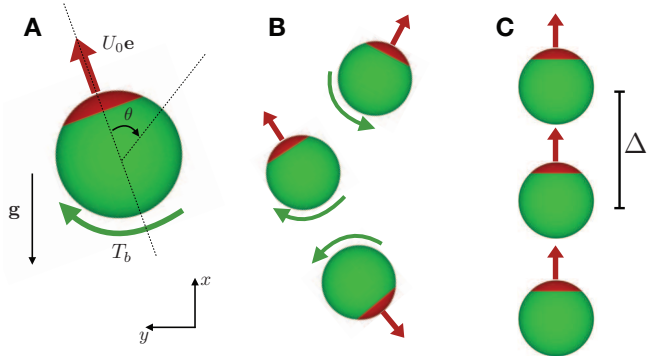

Fig. 1: Numerical setup for our calculations. (A) Squirmers swimming with velocity $U_0\mathbf{e}$ with an anterior side indicated by the small red cap. Swimmer are subject to a restoring torque of magnitude T_b aligning them to swim vertically upward (the angle θ is the polar angle measured from the swimming direction). (B) A suspension of squirmers interact hydrodynamically in a Stokes flow. (C) As initial condition of our simulations the swimmers are aligned along a vertical line and separated by a constant distance Δ.

is the swimming speed of a solitary squirmer and θ is the polar angle measured from $\mathbf{e}$ (see notation in fig. 1). The far-field flow generated by the swimmer is classically given by the dipolar flow [5]

$$\mathbf{u}(\mathbf{r}) = -\frac{3U_0\beta a^2}{4}\left(-\frac{1}{r^3} + \frac{3(\mathbf{e}\cdot\mathbf{r})^2}{r^5}\right)\mathbf{r}, \qquad (1)$$

and the dimensionless parameter β reflects the strength of the force dipole. A squirmer with $\beta > 0$ is a puller, whereas the case with $\beta < 0$ represents that of a pusher.

Due to their bottom heaviness, the squirmers in our model tend to align in the direction opposite to gravity, as illustrated in fig. 1(A). The restoring torque of magnitude T_b is given by $\mathbf{T}_b = \frac{4}{3}\pi a^3\rho h\mathbf{e}\times\mathbf{g}$, where a is the radius of the swimmer, ρ is the density, h is the distance of the centre of mass to the geometric centre of the squirmer, $\mathbf{g}$ is the gravitational acceleration (taken here as $-\mathbf{e}_x$). To measure the effect of bottom heaviness, we can introduce a dimensionless number G_{bh}, defined as $G_{bh} = 4\pi\rho gah/(3\mu U_0)$, where μ is the (dynamic) viscosity of the fluid.

We compute the hydrodynamic interactions between an infinite suspension of squirmers (cf. fig. 1(B)), at negligible particle Reynolds number (*i.e.*, in the absence of inertia), using the Stokesian dynamics method developed in ref. [47]. The far-field contribution to the grand mobility matrix is derived from Faxén's laws. The infinite extent of the suspension is taken into account using Ewald summation [48]. Near-field interactions are added in a pairwise additive fashion using the boundary element method [12]. The method includes an infinite number of reflected far-field interactions among an infinite number of squirmers as well as near-field lubrication forces, whose accuracy was studied in ref. [47]. Further details
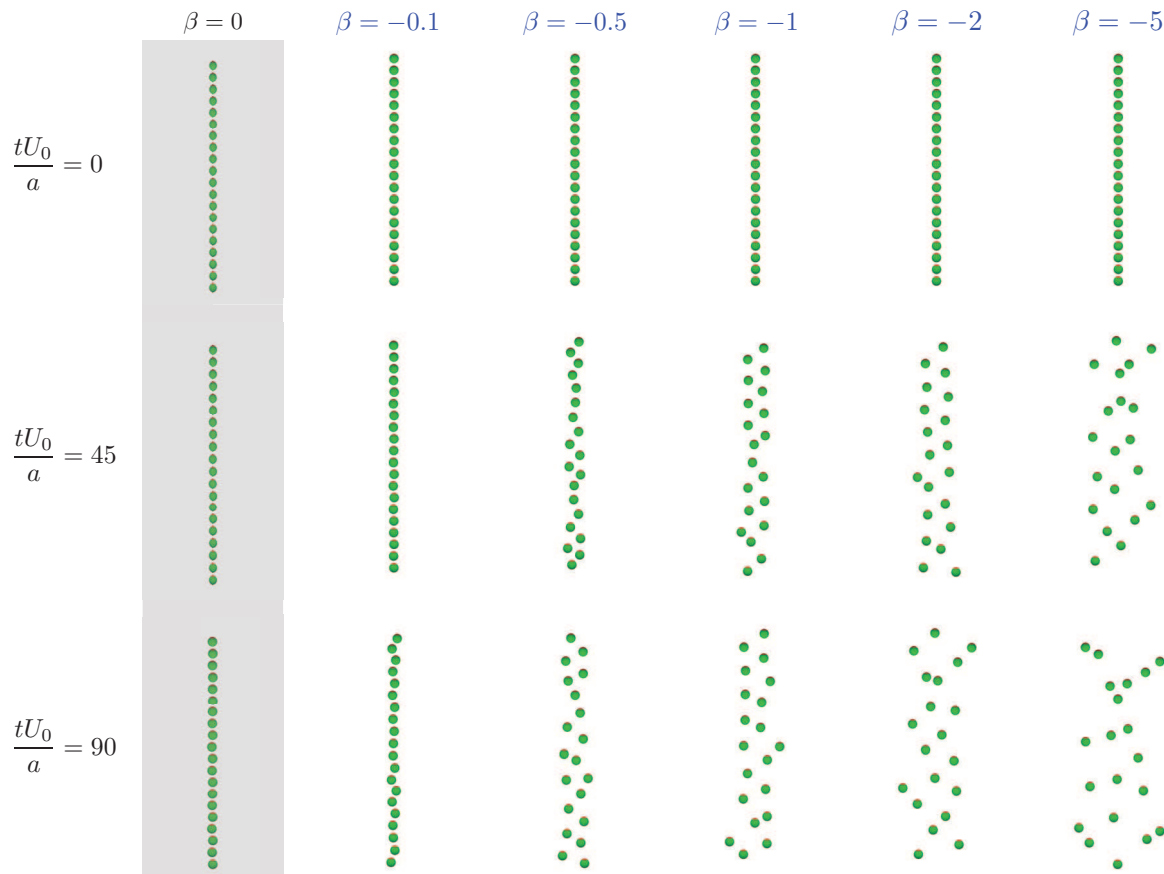
Fig. 2: Numerical results (projected in the x-y plane) showing the initial configuration of swimmers (separation distance $\Delta = 2.5a$) and at the dimensionless times $tU_0/a = 45$ and 90 for five values of the stresslet magnitude: $\beta = 0$ (neutral swimmer) and $\beta = -0.1, -0.5, -1, -2$ and -5 (pushers). We observe a zigzag instability for all pusher swimmers with a growth rate that increases with the magnitude of the dipole parameter, $|\beta|$. Movies of the unstable cases are also available as SM.

on the Stokesian dynamics method are provided in the appendix.

In order to address the stability of a line of swimmers, we place 20 equally distant squirmers along a vertical line, *i.e.*, the x-direction, as shown in fig. 1(C). The initial distance between centres of squirmers is set as $\Delta = 2.5a$, and then small random displacements, less than $0.02a$ in magnitude, are added in the x- and y-directions. The computational domain is a cube with the side length $50a$, and we assume triply periodic boundary conditions. Hence, the line of squirmer is infinitely long in the vertical direction, which is repeated horizontally in the y- and z-directions with $50a$ intervals.

In order to chose a relevant value for G_{bh}, we can turn to past experiments where this dimensionless number can be estimated for *Volvox carteri* colonies [49,50]. The value of G_{bh} depends on the size of the colonies, and ranges from about 1.8 to $G_{bh} \gg 1$ in the case of large colonies (above $300\,\mu$m in size). We therefore consider here squirmers with $G_{bh} = 100$, with orientations that remain almost vertically upward all the time due to the strong bottom heaviness; as long as $G_{bh} \gg 1$, its exact value does not impact our computational results.

Results. We compute numerically the dynamics of the hydrodynamically-interacting pusher squirmers with $\beta = -0.1, -0.5, -1, -2$ and -5, and illustrate our results at dimensionless times $tU_0/a = 0$, 45 and 90 in fig. 2 (movies of these five cases are also available as Supplementary Material (SM): SM_movie_beta-0.1.avi, SM_movie_beta-0.5.avi, SM_movie_beta-1.avi, SM_movie_beta-2.avi, SM_movie_beta-5.avi.). With increasing time, we observe that the initial perturbation grows, and that the squirmers tend to form a zigzag line. After the initial nearly symmetric zigzag growth, the arrangement of squirmers becomes disordered.

The rate of growth of this instability is seen to increase with the magnitude of $|\beta|$, which demonstrates that it is controlled by hydrodynamic interactions between squirmers. We observe the instability in the all pusher cases, *i.e.*, $\beta < 0$ but it disappears in the case of pullers, *i.e.*, $\beta > 0$, where it is instead replaced by the clustering instability reported in ref. [44]. We include in fig. 2 the results in the neutral case $\beta = 0$ (left); in that case the line of swimmer is not unstable.

In order to further quantify the dependence of the instability on the value of the squirmer parameter β, we plot
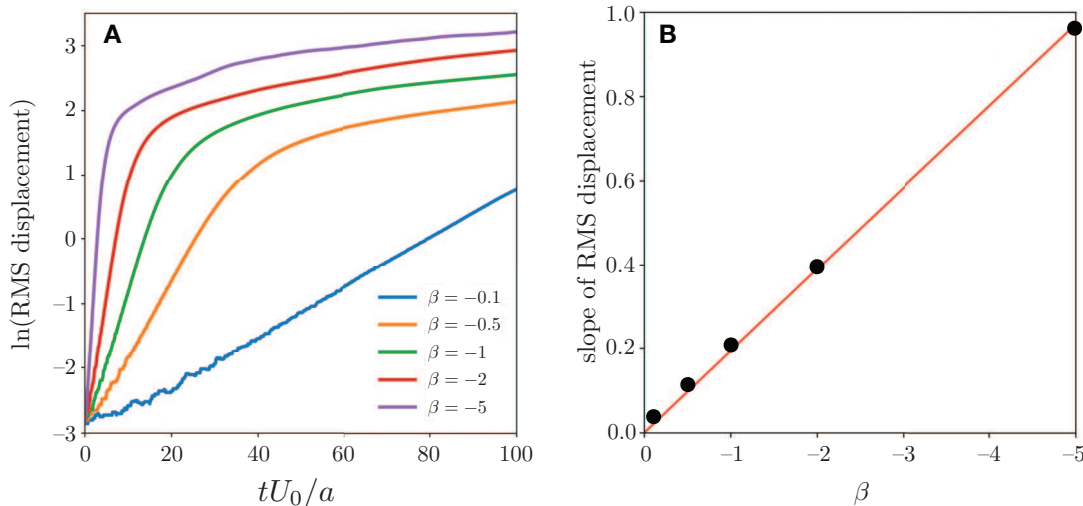
Fig. 3: Exponential growth of the zigzag instabilities as obtained numerically. (A) Time change of the root mean square (RMS) horizontal displacement of the perturbation for different values of β. The plot is displayed using log along y, hence all initial straight slopes indicate exponential growth. (B) Initial exponential growth (obtained from (A) using least squares on the data from $tU_0/a = 0$ to the time at which the RMS displacement becomes one third of its value at $tU_0/a = 100$) as a function of β; the red line is the least-square linear fit passing through origin ($R^2 > 0.99$).

in fig. 3(A) the time dependence of the root mean square (RMS) horizontal displacement of the perturbation for the five values of β. We display the result using a log scale along the y-axis, and thus a linear slope in the figure indicates an exponential growth of the perturbation. Such a linear slope is apparent for all values of β, which clearly illustrates that the instability grows exponentially in all cases.

We next measure the slopes of this exponential growth using least squares on the data ranging from $tU_0/a = 0$ to the time at which the RMS displacement becomes one third of its maximum value in the interval $tU_0/a = 0 \rightarrow 100$. We note that the slope (and thus the growth rate) is essentially constant during this time interval. The fitted growth rates are then plotted as a function of the value of β in fig. 3(B); the red line in the figure is a linear least-square fit passing the origin. Our computational results clearly show that the exponential growth of the instability is proportional to β; the same result will be recovered by the linear stability analysis in the next section.

Finally, in order to determine which wavelength of the initial perturbation grows the fastest in our instability, we calculate the power spectrum of the RMS horizontal displacement at the time $tU_0/a = 3$ as a function of the wavelength (normalised by the initial inter-swimmer distance); the results are then averaged over 10 independent simulations with different initial conditions and plotted in fig. 4. The largest amplitude appears at twice the initial interval, which indicates that the most unstable wavelength is equal to twice the inter-swimmer distance. This result, which is the sign of a zigzag instability, will also be confirmed by the modelling carried out in the next section.

Theoretical model. – Motivated by the computational results shown in fig. 2, in this section we model theoretically the three-dimensional swimmers as stresslets moving on a line. Before the instability, the swimmers are assumed to be located on a one-dimensional lattice of spacing Δ along the x-direction and we assume their orientation is also fixed along x. We know from the work in ref. [44] that pushers are stable to perturbations along x (no clustering mode). Inspired by our numerical results, we then look for an instability due to perturbation in position along y, perpendicular to the direction of swimming (and thus that of the orientation of the cells).

Moving into the co-swimming frame, the far-field flow induced by a cell swimming along a unit vector $\mathbf{e}$ located at the origin is assumed to be given by a stresslet in the form of a force dipole of strength $\mathcal{P}$

$$\mathbf{u}^{\mathcal{P}}(\mathbf{r}) = \frac{\mathcal{P}}{8\pi\mu}\left(-\frac{1}{r^3} + \frac{3(\mathbf{e}\cdot\mathbf{r})^2}{r^5}\right)\mathbf{r}. \qquad (2)$$

Indeed, for the squirmer model used in our simulations, it is a classical result that the flow in the far field is given by eq. (1), *i.e.*,

$$\mathbf{u}(\mathbf{r}) = -\frac{3U_0\beta a^2}{4}\left(-\frac{1}{r^3} + \frac{3(\mathbf{e}\cdot\mathbf{r})^2}{r^5}\right)\mathbf{r}, \qquad (3)$$

which is that of a force dipole, eq. (2), with $\mathcal{P} = -6\pi\mu U_0\beta a^2$. The dipole strength is therefore of the sign opposite to the parameter β in our numerical simulations. We assume the orientation of the swimmers is unchanged and fixed to $\mathbf{e} = \mathbf{e}_x$ so eq. (2) becomes

$$\mathbf{u}^{\mathcal{P}}(\mathbf{r}) = \frac{\mathcal{P}}{8\pi\mu}\left(-\frac{1}{r^3} + \frac{3x^2}{r^5}\right)\mathbf{r}. \qquad (4)$$
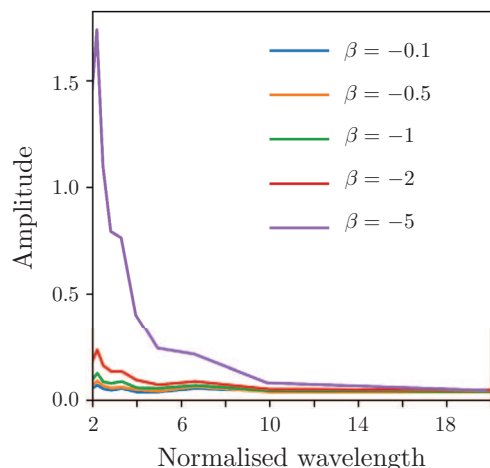
Fig. 4: Power spectrum of the RMS horizontal amplitude at $tU_0/a = 3$ as a function of the wavelength of the perturbation normalized by the initial inter-swimmer distance (equal here to $\Delta = 2.5a$). The results are averaged over 10 independent simulations with different initial conditions and show that the maximum amplitude is obtained for a wavelength equal to twice the inter-swimmer distance.

Here $r^2 = x^2 + y^2 + z^2$ and we restrict in what follows the whole motion to the $z = 0$ plane. Since we investigate stability along the y-direction, we need to evaluate the y-component of the swimmer-swimmer interactions, which is given by

$$u_y^{\mathcal{P}}(x,y) = \frac{\mathcal{P}}{8\pi\mu} \frac{y(2x^2 - y^2)}{r^5}. \qquad (5)$$

Before the instability the swimmers are at the fixed points $\bar{\mathbf{x}}_n = (n\Delta, 0)$. We allow them to be perturbed by ϵ_n along the y-direction with no perturbation along x so that $\mathbf{x}_n = \bar{\mathbf{x}}_n + \delta\mathbf{x}_n = (n\Delta, \epsilon_n)$. Due to hydrodynamic interactions with all other swimmers, and in the absence of inertia, the dynamics of swimmer #n is then given along y by the sum of the y velocities created by all other swimmers #p with $p \neq n$, i.e.,

$$\dot{\epsilon}_n = \sum_{p>1} u_y^{\mathcal{P}}(x_n - x_{n+p}, y_n - y_{n+p}) \\ + \sum_{p>1} u_y^{\mathcal{P}}(x_n - x_{n-p}, y_n - y_{n-p}). \qquad (6)$$

Using a Taylor expansion for small ϵ_n with $\epsilon_n - \epsilon_{n-p} \ll p\Delta$ we have at first order in the ϵ_q's

$$u_y^{\mathcal{P}}(x_n - x_{n-p}, y_n - y_{n-p}) = \frac{\mathcal{P}}{4\pi\mu} \frac{(\epsilon_n - \epsilon_{n-p})}{(p\Delta)^3}. \qquad (7)$$

Assuming nearest-neighbour interactions for simplicity, we next obtain at first order

$$\dot{\epsilon}_n = u_y^{\mathcal{P}}(x_n - x_{n+1}, y_n - y_{n+1}) \\ + u_y^{\mathcal{P}}(x_n - x_{n-1}, y_n - y_{n-1}) \\ = \frac{\mathcal{P}}{4\pi\mu\Delta^3}(2\epsilon_n - \epsilon_{n+1} - \epsilon_{n-1}). \qquad (8)$$

Looking for Fourier modes of the form

$$\epsilon_{n\pm p} = \varepsilon\, e^{\sigma t} e^{-i[k(n\pm p)\Delta]}, \qquad (9)$$

we finally obtain from eq. (8) the dispersion relation for the modes

$$\sigma = \frac{\mathcal{P}}{4\pi\mu\Delta^3}\left(2 - e^{-ik\Delta} - e^{ik\Delta}\right) = \frac{\mathcal{P}}{2\pi\mu\Delta^3}\left(1 - \cos k\Delta\right). \qquad (10)$$

Clearly $\sigma > 0$ for all values of the discrete wavenumber k provided that $\mathcal{P} > 0$, which corresponds to $\beta < 0$ in the simulations. A line of pusher cells swimming along x and also aligned with x leads to an instability along y, i.e., in the direction perpendicular to the direction of swimming. This is consistent with what we observed in our numerical simulations. In contrast, the case of pullers with $\mathcal{P} < 0$ (i.e., $\beta > 0$) is stable, again in agreement with our computational results. Furthermore, we obtain that the growth rate of the instability scales increases linearly with the magnitude of the dipole, a result consistent with the simulations shown in fig. 3.

What is the shape of the most unstable mode, i.e., the one leading to the largest value of σ? For a given value of the dipole strength, the maximum growth rate is obtained for $\cos k\Delta = -1$, i.e., $k\Delta = \pi$. Using eq. (9) we therefore have

$$\epsilon_m = \varepsilon\, e^{\sigma t} e^{-imk\Delta} = \varepsilon\, e^{\sigma t} e^{-im\pi}, \qquad (11)$$

and since $e^{-i\pi} = -1$ this means that

$$\epsilon_m = \varepsilon\, e^{\sigma t}(-1)^m. \qquad (12)$$

The most unstable mode corresponds therefore to alternating $+/-$ transverse motion of the swimmers and the most unstable wavelength is twice the inter-swimmer distance. This is identical to the zigzag motion seen in the numerics (figs. 2 and 4).

Discussion. – The study carried out in this letter is focused on one-dimensional lines of microswimmers. Past theoretical work addressed three-dimensional instability modes coupling orientation and density for swimmer suspensions [34–36]. By tackling swimmers with a fixed orientation, we are able here to focus on position instabilities. A previous calculation showed that pullers are unstable to clustering [44], confirming results seen in numerical simulations [51] and in agreement with the bands of swimmers observed in a previous study [52]. The zigzag instability discovered in the current work is consistent with the results of ref. [52] showing a similar instability arising in an horizontal band of puller swimmers (see their fig. 5). Since a horizontal straight line of pullers have hydrodynamic interactions analogous to a vertical straight line of pushers, both instabilities have the same physical mechanism.

The work in our letter can also be used to explain instabilities in finite-size clusters of swimmers. We illustrate

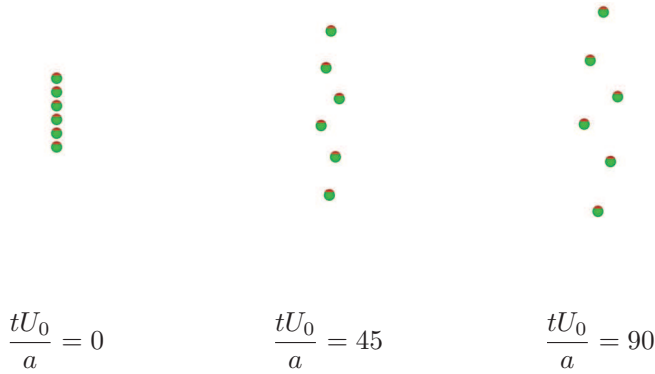$$\frac{tU_0}{a} = 0 \qquad \frac{tU_0}{a} = 45 \qquad \frac{tU_0}{a} = 90$$

Fig. 5: Zigzag instability in the case of a finite suspension of $N = 6$ pusher squirmers with $\beta = -2$. The periodicity of the domain is taken to be $1000a$ in each direction in order to model the dynamics of an isolated cluster. The swimming cells are repelled from one another while displaying the instability.

this by carrying out numerical simulations for a finite suspension of $N = 6$ identical pusher squirmers with $\beta = -2$ in a periodic domain of periodicity $1000a$ in all three directions. The results are shown in fig. 5, with the initial configuration and the positions of the swimmers at three different times (results are shown in the frame of the swimming cluster). Since this is a finite group of swimmers, the pusher flow fields induce a repulsion between the cells and they move away from one another. As this repulsion takes place, we clearly see superimposed the same zigzag instability as in the previous case of the infinite line. An idealised study on an infinite line can therefore provide the basis for understanding the dynamics of finite swimmer clusters.

Summary. – In summary, motivated by the focusing of biased swimmers along thin lines, we investigated theoretically in this letter the stability of a line of biased swimmers. We first used Stokesian dynamics simulations of spherical squirmers with full hydrodynamic interactions to reveal a new zigzag instability in the transverse position of the swimmers, which occurs only in the case of pusher cells. Using a far-field stresslet model, we were then able to rationalise the numerical results, predicting in particular that the most unstable wavelength is equal to twice the inter-swimmer distance and that the growth rate of the instability increases with the magnitude of the stresslet, both of which are agreement with our numerical simulations.

$$* \; * \; *$$

Appendix: Stokesian dynamics. – At negligible particle Reynolds number, the motions of N squirmers periodically replicated in three-dimensional space is solution to [47]

$$\left[\mathbf{I} + \mathbf{M}_{FU}^{far} : \mathbf{K}_{FU}^{2b} \right] \cdot \begin{pmatrix} \mathbf{U} - U_0 \mathbf{e} + \mathbf{H}_{sq} \\ \boldsymbol{\Omega} \end{pmatrix} = \mathbf{M}_{SU}^{far} : \mathbf{S}^{far}$$

$$+ \mathbf{M}_{FU}^{far} \cdot \left\{ \begin{pmatrix} \mathbf{F} + \mathbf{F}^\alpha \\ \mathbf{T} + \mathbf{T}^\alpha \end{pmatrix} - \mathbf{K}_{SU}^{2b} : \left[-\frac{3}{10} U_0 \beta \left(3\mathbf{ee} - \mathbf{I} \right) \right] \right\}, \tag{A.1}$$

with

$$\begin{pmatrix} \mathbf{F}^\alpha \\ \mathbf{T}^\alpha \end{pmatrix} = \mathbf{K}_{2B}^n : \begin{pmatrix} -U_0 \mathbf{e} + \mathbf{H}_{sq} \\ 0 \\ -\frac{3}{10} U_0 \beta \left(3\mathbf{ee} - \mathbf{I} \right) \end{pmatrix} - \begin{pmatrix} \mathbf{F}_{sq}^n \\ \mathbf{T}_{sq}^n \end{pmatrix} \tag{A.2}$$

and

$$\mathbf{M}^{far} = \begin{bmatrix} \mathbf{M}_{FU}^{far} & \mathbf{M}_{FE}^{far} \\ \mathbf{M}_{SU}^{far} & \mathbf{M}_{SE}^{far} \end{bmatrix}, \tag{A.3}$$

$$\mathbf{K}^{2b} = -\mathbf{K}_{2B}^{far} + \mathbf{K}_{2B}^n = \begin{bmatrix} \mathbf{K}_{FU}^{2b} & \mathbf{K}_{FE}^{2b} \\ \mathbf{K}_{SU}^{2b} & \mathbf{K}_{SE}^{2b} \end{bmatrix}, \tag{A.4}$$

where $\mathbf{F}$, $\mathbf{T}$ and $\mathbf{S}$ are, respectively, the force, torque, and stresslet exerted by a squirmer on the fluid; $\mathbf{U}$ and $\boldsymbol{\Omega}$ are the translational and rotational velocities of the squirmer, and $\mathbf{I}$ is the unit tensor; $\mathbf{S}^{far}$ and $\mathbf{H}_{sq}$ are, respectively, the far-field contributions to the stresslet and the irreducible quadrupole, which are approximated by neglecting the additional contribution of cell-cell interactions; $\mathbf{M}^{far}$ is the far-field contribution to the grand mobility matrix derived from Faxén's laws. The infinite extent of the suspension is taken into account using Ewald summation [48]. To include near-field interactions, we add near-field multipoles in a pairwise additive fashion. The far-field two-body resistance matrix is $\mathbf{K}_{2B}^{far}$ while $\mathbf{K}_{2B}^n$ is the near-field two-body resistance matrix. The mobility and resistance matrices are split into four components, as in eq. (A.4), with subscripts FU, FE, SU, and SE indicating couplings between force and velocity, force and rate of strain, stresslet and velocity, and stresslet and rate of strain, respectively. The vectors $\mathbf{F}_{sq}^n$ and $\mathbf{T}_{sq}^n$ are, respectively, the force and torque generated by the two-squirmer interaction in the near field, calculated numerically using the boundary element method [12]. A short-range interparticle repulsive force is added to the system to avoid the prohibitively small time step needed to overcome the problem of overlapping particles [53]. The accuracy of the method was confirmed by two benchmark tests in ref. [47]: i) interaction of three inert spheres in a shear flow, and ii) diffusion of squirmers in a fluid otherwise at rest.

REFERENCES

[1] BRAY D., *Cell Movements* (Garland Publishing, New York, NY) 2000.
[2] TAYLOR G. I., *Proc. R. Soc. A*, **209** (1951) 447.
[3] PURCELL E. M., *Am. J. Phys.*, **45** (1977) 3.
[4] LIGHTHILL J., *Mathematical Biofluiddynamics* (SIAM, Philadelphia) 1975.
[5] LAUGA E., *The Fluid Dynamics of Cell Motility* (Cambridge University Press, Cambridge, UK) 2020.
[6] MARCHETTI M. C., JOANNY J.-F., RAMASWAMY S., LIVERPOOL T. B., PROST J., RAO M. and SIMHA R. A., *Rev. Mod. Phys.*, **85** (2013) 1143.
[7] BATCHELOR G. K., *J. Fluid Mech.*, **41** (1970) 545.
[8] DRESCHER K., GOLDSTEIN R. E., MICHEL N., POLIN M. and TUVAL I., *Phys. Rev. Lett.*, **105** (2010) 168101.
[9] DRESCHER K., DUNKEL J., CISNEROS L. H., GANGULY S. and GOLDSTEIN R. E., *Proc. Natl. Acad. Sci. U.S.A.*, **108** (2011) 10940.
[10] KLINDT G. S. and FRIEDRICH B. M., *Phys. Rev. E*, **92** (2015) 063019.
[11] GUASTO J. S., JOHNSON K. A. and GOLLUB J. P., *Phys. Rev. Lett.*, **105** (2010) 168102.
[12] ISHIKAWA T., SIMMONDS M. P. and PEDLEY T. J., *J. Fluid Mech.*, **568** (2006) 119.
[13] HERNANDEZ-ORTIZ J. P., STOLTZ C. G. and GRAHAM M. D., *Phys. Rev. Lett.*, **95** (2005) 204501.
[14] ISHIKAWA T., SEKIYA G., IMAI Y. and YAMAGUCHI T., *Biophys. J.*, **93** (2007) 2217.
[15] LAUGA E. and BARTOLO D., *Phys. Rev. E*, **78** (2008) 030901.
[16] LAUGA E. and GOLDSTEIN R. E., *Phys. Today*, **65**, issue No. 9 (2012) 30.
[17] KOCH D. L. and SUBRAMANIAN G., *Annu. Rev. Fluid Mech.*, **43** (2011) 637.
[18] SAINTILLAN D., *Annu. Rev. Fluid Mech.*, **50** (2018) 563.
[19] PALACCI J., SACANNA S., STEINBERG A. P., PINE D. J. and CHAIKIN P. M., *Science*, **339** (2013) 936.
[20] DOMBROWSKI C., CISNEROS L., CHATKAEW S., GOLDSTEIN R. E. and KESSLER J. O., *Phys. Rev. Lett.*, **93** (2004) 098103.
[21] CISNEROS L. H., CORTEZ R., DOMBROWSKI C., GOLDSTEIN R. E. and KESSLER J. O., *Exp. Fluids*, **43** (2007) 737.
[22] SOKOLOV A., ARANSON I. S., KESSLER J. O. and GOLDSTEIN R. E., *Phys. Rev. Lett.*, **98** (2007) 158102.
[23] WOLGEMUTH C. W., *Biophys. J.*, **95** (2008) 1564.
[24] SOKOLOV A. and ARANSON I. S., *Phys. Rev. Lett.*, **109** (2012) 248109.
[25] COPELAND M. F. and WEIBEL D. B., *Soft Matter*, **5** (2009) 1174.
[26] DARNTON N. C., TURNER L., ROJEVSKY S. and BERG H. C., *Biophys. J.*, **98** (2010) 2082.
[27] CHILDRESS S., LEVANDOWSKY M. and SPIEGEL E. A., *J. Fluid Mech.*, **69** (1975) 591.
[28] HILL N. A. and PEDLEY T. J., *Fluid Dyn. Res.*, **37** (2005) 1.
[29] RIEDEL-KRUSE I. H. and HOWARD J., *Science*, **309** (2005) 300.
[30] LIAO Q., SUBRAMANIAN G., DELISA M. P., KOCH D. L. and WU M. M., *Phys. Fluids*, **19** (2007) 061701.
[31] BASKARAN A. and MARCHETTI M. C., *Proc. Natl. Acad. Sci. U.S.A.*, **106** (2009) 15567.
[32] CATES M. E. and TAILLEUR J., *Annu. Rev. Condens. Matter Phys.*, **6** (2015) 219.
[33] DRAZIN P. G. and REID W. H., *Hydrodynamic Stability* (Cambridge University Press) 2004.
[34] SIMHA R. A. and RAMASWAMY S., *Phys. Rev. Lett.*, **89** (2002) 058101.
[35] SAINTILLAN D. and SHELLEY M. J., *Phys. Fluids*, **20** (2008) 123304.
[36] HOHENEGGER C. and SHELLEY M. J., *Phys. Rev. E*, **81** (2010) 046311.
[37] DRISCOLL M., DELMOTTE B., YOUSSEF M., SACANNA S., DONEV A. and CHAIKIN P., *Nat. Phys.*, **13** (2017) 375.
[38] PEDLEY T. J. and KESSLER J. O., *Annu. Rev. Fluid Mech.*, **24** (1992) 313.
[39] JÉKELY G., *Phil. Trans. R. Soc. B*, **364** (2009) 2795.
[40] WILLIAMS C. and BEES M., *J. Fluid Mech.*, **678** (2011) 41.
[41] KELLER E. F. and SEGEL L. A., *J. Theor. Biol.*, **30** (1971) 225.
[42] BERG H. C., *E. coli in Motion* (Springer-Verlag, New York, NY) 2004.
[43] KESSLER J. O., *Nature*, **313** (1985) 218.
[44] LAUGA E. and NADAL F., *EPL*, **116** (2017) 64004.
[45] LIGHTHILL M. J., *Commun. Pure Appl. Math.*, **5** (1952) 109.
[46] BLAKE J. R., *J. Fluid Mech.*, **46** (1971) 199.
[47] ISHIKAWA T., *J. Fluid Mech.*, **705** (2012) 98.
[48] BEENAKKER C. W. J., *J. Chem. Phys.*, **85** (1986) 1581.
[49] DRESCHER K., LEPTOS, K. C. and TUVAL I., ISHIKAWA T., PEDLEY T. J. and GOLDSTEIN R. E., *Phys. Rev. Lett.*, **102** (2009) 168101.
[50] ISHIKAWA T., PEDLEY T. J., DRESCHER K. and GOLDSTEIN R. E., *J. Fluid Mech.*, **903** (2020) A111.
[51] JIBUTI L., QI L., MISBAH C., ZIMMERMANN W., RAFAI S. and PEYLA P., *Phys. Rev. E*, **90** (2014) 063019.
[52] ISHIKAWA T. and PEDLEY T. J., *Phys. Rev. Lett.*, **100** (2008) 088103.
[53] ISHIKAWA T., LOCSEI J. T. and PEDLEY T. J., *J. Fluid Mech.*, **615** (2008) 401.